HYPERFINE STRUCTURE CONSTANTS FOR LEVELS OF $^{175}Lu^{+}$

(short title: $^{175}Lu^{+}$ HYPERFINE STRUCTURE)

E. A. Den Hartog[1], J. E. Lawler[1] and I. U. Roederer[2,3]

[1]Department of Physics, University of Wisconsin-Madison, 1150 University Ave, Madison, WI 53706; eadenhar@wisc.edu; jelawler@wisc.edu

[2]Department of Astronomy, University of Michigan, 1085 S. University Ave., Ann Arbor, MI 48109, USA; iur@umich.edu

[3]Joint Institute for Nuclear Astrophysics – Center for the Evolution of the Elements (JINA-CEE), USA

Abstract

Accurate and complete atomic data are required for the determination of accurate stellar photospheric abundances. This includes hyperfine structure for some elements – those with high nuclear spin and/or large nuclear magnetic moments. Lutetium is one such element. In this study, spectra of a commercial Lu-Ne hollow cathode lamp operating at low current were recorded with the high-resolution University of Wisconsin 3-m focal length echelle spectrograph. These spectra of resolved and partially resolved hyperfine patterns for 35 UV and blue transitions of Lu II have been studied for the purpose of extracting hyperfine constants. We present hyperfine structure constants for 16 levels of singly-ionized lutetium, 10 of which have been measured for the first time.

1. INTRODUCTION

Metal-poor (MP) stars are the most ancient population of stars in the Milky Way Galaxy. These stars contain fossil records of the conditions in the interstellar environment when and where they formed. The study of rare earth and other heavy element abundances in MP stars give us a glimpse into nucleosynthesis events that occurred very early in the history of the universe. Some fraction of MP stars have significantly enhanced abundances of elements produced via the *r*(apid)-process *n(*eutron)-capture (e.g., Sneden et al. 1996; Barklem et al. 2005; Hansen et al. 2018). Accurate abundance determinations in such stars often require ultraviolet (UV) data from the *Hubble Space Telescope*. The use of low excitation potential UV lines to ground and low metastable levels of the ion has important advantages, since an overwhelming fraction of all heavy elements in the photospheres of MP stars exists in singly-ionized form. Thus, the ground and low metastable levels (if such levels exist) of the ion typically serve as reservoir levels for the element in the photosphere. Populations of ion reservoir levels are generally close to local thermodynamic equilibrium (LTE), but many lines in minor species (e.g. the neutral atom) yield abundance values only after applying large and uncertain non-LTE corrections. Non-LTE photospheric models are being developed (e.g. Asplund 2005; Asplund et al. 2009; Amarsi et al. 2018, 2019a, 2019b), but many accurate and precise rate constants are needed to make such models generally reliable. Important progress on the needed rate constants for some species is being made (e.g. Barklem et al. 2011; Barklem 2016, 2017, 2018a, 2018b).

Accurate and complete atomic data are also required for accurate abundance determinations. The use of laser induced fluorescence has much improved experimental log(*gf*)s over the last few decades, but observers need more than reliable transition probabilities to extract abundance values from stellar spectra. If an absorption line of interest is saturated, then hyperfine structure (HFS) and/or isotope shifts are needed. Although HFS is generally unresolved in stellar spectra due to wide Doppler widths at photospheric temperature, it is important to include this structure to reliably desaturate the line. Lutetium is the least abundant of the rare earths, and it has proved to be a challenge to determine reliable MP star abundances from Lu II lines in the optical and near-UV (see, for example, the discussion in Sneden et al. 2009). More success is likely to be had in *r*-process enhanced MP stars due to the higher abundances. The current study is motivated by a detection of the Lu II line in the far-UV at 2195.56 Å in the MP star HD 196944 (I.U. Roederer et al., in preparation), which should help confirm abundances derived from other Lu II lines in the UV spectral range (e.g., Roederer et al. 2010, 2012; Placco et al. 2015).

Lutetium, Z=71, has two stable isotopes, A=175 and 176[4]. In the solar system the vast majority (97.4%) is ^{175}Lu, which has nuclear spin I = 7/2 and relatively large nuclear magnetic dipole moment (~+2.23 nuclear magnetons) and electric quadrupole moment (~+3.5 barnes) (Stone 2005). These properties give rise to substantial HFS, which is clearly discernible for most lines in high-resolution laboratory spectra in the optical and UV. The small 2.6% contribution from the ^{176}Lu isotope can usually be neglected, and has been mostly neglected in the present study. The minor isotope was barely detected on a single line as described in §2 below.

[4] ^{176}Lu is not technically stable, but has a half-life of 3.6×10^{10} years (Stone 2005)

Some work on the HFS of Lu II can be found in the literature. Brix & Kopfermann (1952) summarized Lu II HFS to-date, reporting *A*'s and *B*'s for five low-lying levels of the 5*d*6*s* and 6*s*6*p* configurations from various sources. Values for these same levels were reported a few years later with higher accuracy (Steudel 1958). *A* and *B* coefficients for two levels, the 5*d*6*s* $^3D_1$ and 6*s*6*p* $^3P^o_1$, were confirmed by our University of Wisconsin – Madison (UW) group (Den Hartog et al. 1998). We subsequently made a more extensive HFS analysis of Lu II (Sneden et al. 2003, hereafter Sn03), reporting HFS *A*'s and *B*'s and improved energies for ten levels including the five reported by Brix & Kopfermann and Steudel as well as five additional levels from the 6*s*6*p* and 5*d*6*p* configurations. In the current study we repeat measurements for six of the levels studied by Sn03 to validate our technique using a different spectrometer (see discussion in §2 below) and report HFS constants for an additional ten levels. The fitting software used in the current study is largely the same as used by Sn03.

2. EXPERIMENT

The most accurate HFS measurements for levels above the ground term are made using Doppler-free laser techniques. These experiments tend to be expensive and time consuming. Alternatively, many HFS studies are carried out using high-resolution emission measurements of hollow cathode lamps (HCLs). This is an effective technique in cases where the structure is spread over a range much larger than the Doppler widths of the emission lines. Often a Fourier Transform Spectrometer (FTS) is used for studies of this type due to their high resolving power, broad wavelength coverage and absolute wave number accuracy. The earlier studies our group performed on the HFS of Lu II (Den Hartog et al. 1998; Sn03) utilized spectra of Lu-Ar and Lu-Ne commercial sealed HCLs taken with the 1-m FTS at the National Solar Observatory (NSO) at Kitt Peak, AZ. This (now decommissioned) instrument had the advantages listed above, but was not ideally suited to work far into the UV, as the sensitivity rolled off substantially at wave numbers above 25000 cm^{-1}. It also shares the shortcoming of all interferometric devices in that the Poisson statistical noise from all lines in the spectrum is redistributed evenly throughout the spectrum. Referred to as multiplex noise, it makes work on weak lines difficult. Hyperfine patterns often combine strong and weak components. If one needs to turn up the lamp current in order to bring the weak components out of the noise, there is the risk of optical depth on the strong components, and the relative intensities will not fit to theory (see, for example, discussion of Figure 2 in Özdalgiç, Başar & Kröger 2019).

This study utilizes the UW 3-m focal length echelle spectrograph (Wood & Lawler 2012). The instrument has a large (128×254 mm ruled area), coarse (23.2grooves/mm) echelle grating blazed at 63.5°. It operates in very high orders (up to order m=385 at 2000 Å) resulting in a high resolving power (up to ~300,000) and has good sensitivity down to 2000 Å. As a dispersive instrument it is free from multiplex noise, and therefore suited for measuring even weak lines with good signal-to-noise (S/N). The UW 3-m was originally developed for the purpose of measuring weak, UV branching fractions of the iron-group elements and has been deployed in a number of successful studies on transition probabilities of: Ti I (Lawler et al. 2013); Ti II (Wood et al. 2013); V II (Den Hartog et al. 2014; Wood et al. 2014a); Ni I (Wood et al. 2014b); V I

(Lawler et al. 2014; Wood et al. 2018); Co I (Lawler et al. 2015); Cr II (Lawler et al. 2017), Co II (Lawler et al. 2018), Sc I,II (Lawler et al. 2019) and Fe II (Den Hartog et al. 2019). In the work reported here, this instrument was used to record low current emission spectra from a commercial sealed lutetium HCL. These commercially available HCLs are convenient to use and operate very stably and quietly. The lamp used contains neon as the buffer gas and was run at 20 mA DC current. No evidence of optical depth was observed in any of the transitions studied. Unfortunately, this HCL also produced contaminant lines, primarily of Fe I and II, which increased the potential for blends substantially.

The 3-m echelle has a high resolving power but does not match the resolving power or absolute wavelength accuracy of the NSO 1-m FTS or similar research instruments. The usual mode of operation for branching fraction work utilizes a 50 μm entrance pinhole. The exit plane is then imaged onto a 2048×2048 Charge Coupled Device (CCD) detector after passing through a prismatic order separator. The order separator is designed such that it largely eliminates the primary aberration of the main instrument, which is astigmatism. Residual field curvature results in only the center of the CCD being in perfect focus, with the focus degraded toward the CCD edges. For branching fraction work, where the entire CCD is used, a compromise focus results in good resolving power (~250,000) over the entire CCD. For the current study, we needed the best possible resolving power, so we operated with a 10 μm entrance pinhole and sharpened the focus at the center of the CCD. Only the central ~1/5 of the CCD was used. A single or sometimes closely spaced pair of lines were moved to the central position by rotating the grating of the 3-m and the prism of the order separator. Individual HFS patterns are extracted from these spectra by summing the intensities in pixels across the width of the order in which the transition is found (usually about 6-8 pixels). The resolving power under these conditions is ~300,000.

Figure 1 illustrates how the spectral integrity of the 3-m echelle compares to that of the 1-m FTS used in the earlier study of Sn03. This figure shows the fully-resolved $^3P_1 - {}^1S_0$ transition at 28503.16 cm^{-1} (3507.39 Å). The effective resolving power of the FTS, which results from the convolution of the Doppler profile and the instrument profile, is ~360,000 – somewhat better than the 3-m echelle. However, the echelle spectrum has superior S/N, and the ringing seen in the FTS spectrum obscures small features such as the weak lines seen on either side of the triplet in the 3-m echelle spectrum. These weak lines belong to the ^{176}Lu isotope (2.6% isotopic fraction). While we do not have adequate resolution to determine the A and B of this line for this isotope, it is indicative of the good S/N of the echelle that we can distinguish these components. This line at 28503.16 cm^{-1} is the only one for which we have definitively identified the contribution from ^{176}Lu.

A non-linear least-square fit was performed on each transition studied to determine the A_u and B_u of the upper level. The lower level constants, A_l and B_l, were fixed in the fit using the values from Sn03 or $A_l = B_l = 0$ for transitions that connect to a J=0 lower level, which has no HFS. An exception to this is the transition at 38167.34 cm^{-1} (2619.26 Å). In this case the upper level has J=0 and the fit to the HFS pattern is used to (re)determine the hyperfine constants for the lower level, 11796.24 cm^{-1}. **The parameters used in the fit were the HFS A and B, line center-of-gravity wavenumber, total line intensity and the sub-component width parameter, W. The**

relative strengths of sub-components are fixed to the theoretical intensities. The asymmetry of the instrument profile evident in Figure 1 arises due to imperfection in the imaging of the order separator and has some potential to add systematic uncertainty in the determination of our HFS *A*'s and *B*'s. Each HFS sub-component is therefore modeled as the sum of three Gaussians in order to approximate this asymmetry. The central peak of width *W* is fixed as 70% of the total intensity. A second peak of width 2*W* is fixed as 23% of the total intensity and is positioned 0.5*W* toward the blue, and a third peak of width 4W is fixed at 7% of the total intensity, and positioned 0.75*W* to the blue. This asymmetric sub-component profile significantly reduces the potential for systematic effects in the analysis, particularly in cases where the components are not well-resolved. In similar HFS studies using an FTS, such as that carried out by Sn03, the center-of-gravity determined in the fit can be used to improve the accuracy of the energy levels. Although Sn03 did not report improved energy levels, their analysis was later used by Lawler et al. (2009) to report improved energies for the 12 levels involved in the Sn03 study. The lower accuracy of the absolute wavenumber calibration of the 3-m echelle spectrograph means that we cannot improve energy levels as part of the current study.

Table 1 lists all of the transitions utilized in the current study arranged by term-ordered upper level energy**. In this table, energy levels listed to three digits past the decimal are updated values from Lawler et al. (2009) and those listed to one or two digits past the decimal are taken from the National Institute of Standards and Technology Atomic Spectra Database (NIST ASD)[5] (Kramida et al. 2018). If updated level energies from Lawler et al. are available for both levels of a transition, these values are listed in Table 1 and were used to calculate the transition wavenumber. In the cases where only the lower level energy has an updated value, we use the older level energies taken from the NIST ASD for both upper and lower levels. This is to avoid introducing an offset in the calculated transition wavenumber. Therefore, in some instances slightly different values appear in Table 1 for the same level.**

The final column of Table 1 gives a descriptor indicating how well-resolved the line is and whether it contains any blends**. The descriptors are as follows: f – fully resolved, indicates that all components are completely resolved from one another; m – mostly resolved, indicates three or more well-defined peaks with ratio of peak intensity to adjacent minima of two or greater; p – partially resolved, indicates some resolved structure but with less definition than for m; u – unresolved, indicates no resolved structure; bl – blend. Examples of lines that are assigned each descriptor are shown in Figure 2.** In this figure the black "+" symbols indicate the experimental data. The blue line is the non-linear least-squares fit to the data and the black vertical bars show the position and relative intensities of the HFS components calculated in the fit. The red line in panel (a) indicates the position and intensities of the $^{176}Lu^{+}$ isotopic contribution based on the findings of Steudel (1958).[6] Panel (b) also shows

[5] http://physics.nist.gov/asd

[6] Steudel (1958) determined ^{176}A=134.44±0.15, ^{176}B=-86.6±1.1 based on ^{176}I=6. ^{176}I is now known to be 7 (Stone 2005) so the *A* and *B* would need to be adjusted accordingly.

an example of a blend which adds intensity to the second peak from the left. The line was successfully fitted using only the four right-most peaks.

Although the asymmetric instrumental profile, along with the slightly lower resolving power and less accurate wavelengths or wavenumbers are all disadvantages of the 3-m echelle spectrograph compared to FTS instruments, the absence of multiplex noise in spectra from the echelle spectrograph is a more significant advantage over FTS instruments. Many weaker transitions unobserved in earlier FTS studies were observed with satisfactory S/N using the 3-m echelle using similar low current HCLs.

3. RESULTS AND DISCUSSION

Table 2 contains the newly determined hyperfine A's and B's and their associated uncertainties as well as those of Sn03 and Steudel (1958) for the levels where the studies overlap. The HFS constants from Table 2, combined with HFS results from Sn03, are used to generate complete line component patterns for the 35 transitions of Lu II that appear in Table 1. These are presented in machine-readable form in Table 3. In this table we use the Sn03 A's and B's for all levels under 45000 cm^{-1} (except the level near 38223 cm^{-1} which was not included in the Sn03 study) as their results are somewhat more accurate than those from the current study. Note that for the new upper levels of the current study, the center-of-gravity of the line is calculated from the energy levels in the NIST ASD (Kramida et al. 2018). The center-of-gravity of transitions for which both upper and lower levels were studied by Sn03 are calculated from their improved energy levels which were reported in Lawler et al (2009).

The absolute wavelength accuracy of the 3-m echelle is inferior to that of an FTS. However, in determining HFS constants it is the accuracy of relative wavelengths (i.e., line spacing) that is important. In order to assess the accuracy of our relative wavelength calibration, we take advantage of the presence of Fe I and II lines in the spectrum. Ritz wavelengths for these species are very well known. The NIST ASD (Kramida et al. 2018) quotes uncertainties generally in the range 0.5–2x10^{-4} Å in the UV. We chose a pair of Fe I lines in a single order near the center of the CCD spectrum and separated by a few hundred pixels. These lines were then fit with the same non-linear least-squares fitting routine used for the HFS analysis, but modified to fit a pair of lines of arbitrary relative intensity. The position and intensity of each line as well as the line width were the fitting parameters. The relative position determined from the fit was compared to the accurately-known wavelength separation and was used to assess the wavelength calibration uncertainty. This procedure was repeated for three representative CCD frames that span the breadth of the wavelength calibration. In each case the line splitting reproduced to within ~0.1%.

Another source of uncertainty in the A_u's and B_u's determined from the fit are the uncertainties of the A_l and B_l taken from Sn03 that are fixed during the fit. In order to assess the magnitude of these uncertainties the fits were rerun with A_l changed to $A_l+\Delta A_l$ and $A_l-\Delta A_l$ where ΔA_l is the uncertainty reported by Sn03. Independently the same process was done with the B_l

uncertainties. Not surprisingly, changing A_l has a larger effect than changing B_l. We find that a change of A_l by ΔA_l leads to a change in A_u ranging from 0.2 – 2 times ΔA_l with the largest effects for lines where J_u-J_l = -1. The A_u are relatively insensitive to changing B_l by its uncertainty. The B_u were also more sensitive to changes in A_l than to changes in B_l, but since ΔB_l is an order of magnitude larger than ΔA_l, the absolute magnitude of the uncertainty in B_u due to changing B_l by ΔB_l is larger, with ΔB_u ranging from ~0.1 – 2.5 times ΔB_l. The magnitude of these changes were added in quadrature along with the uncertainty in the wavelength calibration to produce a lower bound for the uncertainty in A_u and B_u for each transition.

Contributions to the uncertainties that arise due to complex and/or unresolved structure is more difficult to assess. A pattern such as that in Figure 2(a), which is fully resolved and has no HFS in the lower level has lower relative uncertainty than those illustrated in panels (d) and (e), for example, which have more complex and less resolved structure. In cases where we have studied more than one transition from an upper level, we use the level of agreement between individual fits as a guide, weighting results from better resolved lines more heavily than results from less well-resolved lines and increasing the error bar of the final result when indicated. In a few cases, the hyperfine B's from analysis of multiple transitions have a very poor level of agreement and we chose not to report a B for that level. The good level of agreement with the results of earlier studies also gives some measure against which to judge uncertainties.

4. SUMMARY

We have measured hyperfine constants for 16 levels of singly-ionized lutetium, ten of them for the first time. These constants were determined from the analysis of HFS patterns of 35 Lu II transitions from low current, optically thin spectra recorded on the UW 3-m echelle spectrograph. These HFS constants are used to generate complete line component patterns for the transitions studied which will aid stellar spectroscopists to incorporate the new data into their spectral synthesis codes.

ACKNOWLEDGEMENTS

This work is supported by NSF grant AST1814512 (E.D.H. and J.E.L) and NASA grants NNX16AE96G, HST-GO-15657.004-A (J.E.L.) and HST-GO-14765.001-A (I.U.R.).

REFERENCES

Amarsi, A. M., Barklem, P. S., Asplund, M., Collet, R. & Zatsarinny, O. 2018 A&A 616, A89

Amarsi, A. M., Barklem, P. S., Collet, R., Grevesse, N. & Asplund, M. 2019b A7A 624, A111

Amarsi, A. M., Nissen, P. E., Asplund, M., Lind, K. & Barklem, P. S. 2019a A&A 622, L4

Asplund, M. 2005, ARA&A **43**, 481

Asplund, M., Grevesse, N., Sauval, A. J., & Scott, P. 2009, ARA&A 47, 481

Barklem, P.S. 2016, Phys. Rev. A 93, 0042705

Barklem, P. S. 2017, Phys. Rev. A 95,069906(E)

Barklem, P. S. 2018a, A&A 610, A57

Barklem, P. S. 2018b, A&A 612, A90

Barklem, P.S., Belyaev, A.K., Guitou, M., et al. 2011, Astron. Astrophys. 530, A94

Barklem, P. S., Christlieb, N., Beers, T. C., et al. 2005, Astron. Asrophys., 439, 129

Brix, P., & Kopfermann, H. 1952, Zahlenwerte und Funktionen aus Physik, Chemie, Astronomie, Geophysik und Technik, Landolt-Boernstein, Vol. 1, Part 5, ed. A. Eucken (6th ed.; Berlin: Springer)

Den Hartog, E. A., Curry, J. J., Wickliffe, M. E. & Lawler, J. E. 1998, Solar Physics 178, 239.

Den Hartog, E. A., Lawler, J. E., Sneden, C., Cowan, J. J. & Brukhovesky, A. 2019, ApJS 243, 33.

Den Hartog, E. A., Lawler, J. E. & Wood, M. P. 2014, ApJS 215, 7.

Hansen, T. T., Holmbeck, E. M., Beers, T. C., et al. 2018, ApJ, 858, 92

Kramida, A., Ralchenko, Yu., Reader, J., & NIST ASD Team (2018). *NIST Atomic Spectra Database* (ver. 5.6.1), [Online]. Available: https://physics.nist.gov/asd. National Institute of Standards and Technology, Gaithersburg, MD. DOI: https://doi.org/10.18434/T4W30F

Lawler, J. E., Feigenson, T., Sneden, C., Cowan, J. J., & Nave, G. 2018, ApJS, 238, 7

Lawler, J. E., Guzman, A., Wood, M. P., et al. 2013, ApJS, 205, 11

Lawler, J. E., Hala, Sneden, C., Nave, G., Wood, M. P., & Cowan, J. J. 2019, ApJS, 241, 21

Lawler, J. E., Sneden, C., & Cowan, J. J. 2015, ApJS, 220, 13

Lawler, J. E., Sneden, C., Cowan, J. J., Ivans, I. I., & Den Hartog, E. A. 2009, ApJS, 182, 51

Lawler, J. E., Sneden, C., Nave, G., Den Hartog, E. A., Emrahoğlu, N., & Cowan, J. J. 2017, ApJS 228, 10

Lawler, J. E., Wood, M. P., Den Hartog, E. A., et al. 2014, ApJS 215, 20

Özdalgiç, B., Başar, Gö. & Kröger, S. 2019, ApJS 244, 41

Peck, E. R., & Reeder, K. 1972, JOSA, 62, 958

Placco, V. M., Beers, T. C., Ivans, I. I., et al. 2015, ApJ, 812, 109

Roederer, I. U., Lawler, J. E., Sobeck, J. S., et al. 2012, ApJS, 203, 27

Roederer, I. U., Sneden, C., Lawler, J. E., Cowan, J. J. 2010, ApJL, 714, L123

Sneden, C., Cowan, J. J., Lawler, J. E., et al. 2003, ApJ 591, 936

Sneden, C., Lawler, J. E., Cowan, J. J., Ivans, I. I., & Den Hartog, E. A. 2009 ApJS 182, 80

Sneden, C., McWilliam, A., Preston, G. W., et al. 1996, ApJ, 467, 819

Steudel. A. 1958 Z. Physik 152, 599

Stone, N. J. 2005 At. Data Nuclear Data Tables 90, 75 (2005)

Wood M.P. & Lawler J.E. 2012, Appl. Opt. 51, 8407

Wood, M. P., Lawler, J. E., Den Hartog E. A., et al. 2014a, ApJS, 214, 18

Wood, M. P., Lawler, J. E., Sneden, C., & Cowan, J. J. 2013, ApJS, 208, 27

Wood, M. P., Lawler, J. E., Sneden, C., & Cowan, J. J. 2014b, ApJS, 211, 20

Wood, M. P., Sneden, C., J. E. Lawler, et al. ApJS, 2018, 235, 25

FIGURE CAPTIONS

Figure 1. Comparison of a 1-m NSO FTS spectrum (top panel) and a 3-m echelle spectrum (bottom panel) for the fully resolved line at 28503.1 cm^{-1}. The effective resolving power of the FTS is somewhat superior but the S/N of the 3-m echelle is a significant advantage. **Weak peaks to the red and blue of the line are obvious in the echelle data, but are obscured by ringing in the FTS data. These peaks are the ΔF=±1 HFS components of the $^{176}Lu^{+}$ isotope.**

Figure 2. Examples of hyperfine patterns. In all panels the black + signs indicate the measured 3-m echelle spectrograph data. The blue line is the non-linear least-squares fit to the experimental data. The black vertical lines show relative intensity of the hyperfine sub-components determined in the fit. (a) the fully resolved line at 28503.1 cm^{-1}. Although the fit is only performed for the lines of $^{175}Lu^{+}$, the red line indicates the approximate intensity and line positions for the $^{176}Lu^{+}$ isotope. (b) the mostly resolved line at 35271.1cm^{-1} with a blend in the second component from the left. The fit, indicated by the blue line, is performed on the four components to the right. The black dashed line is the calculated spectrum in the blended region based on the fit. (c) the mostly resolved line at 34337.8 cm^{-1} (d) the partially resolved line at 32483.4 cm^{-1} and (e) the unresolved line at 41789.8 cm^{-1}.

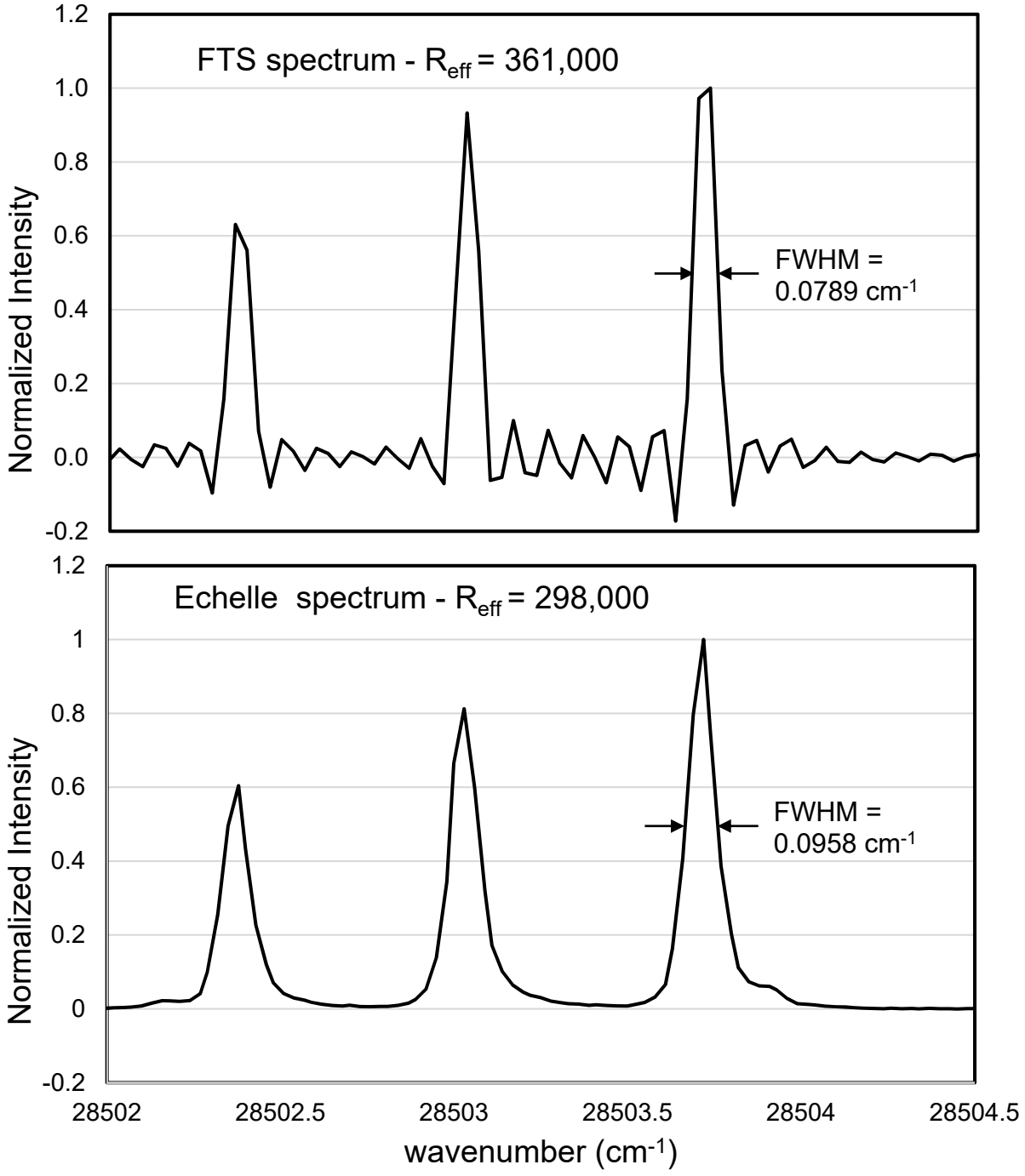
FTS spectrum - R_{eff} = 361,000
FWHM = 0.0789 cm^{-1}
Normalized Intensity
1.2
1.0
0.8
0.6
0.4
0.2
0.0
-0.2
Echelle spectrum - R_{eff} = 298,000
FWHM = 0.0958 cm^{-1}
Normalized Intensity
1.2
1
0.8
0.6
0.4
0.2
0
-0.2
28502
28502.5
28503
28503.5
28504
28504.5
wavenumber (cm^{-1})

Figure 1.

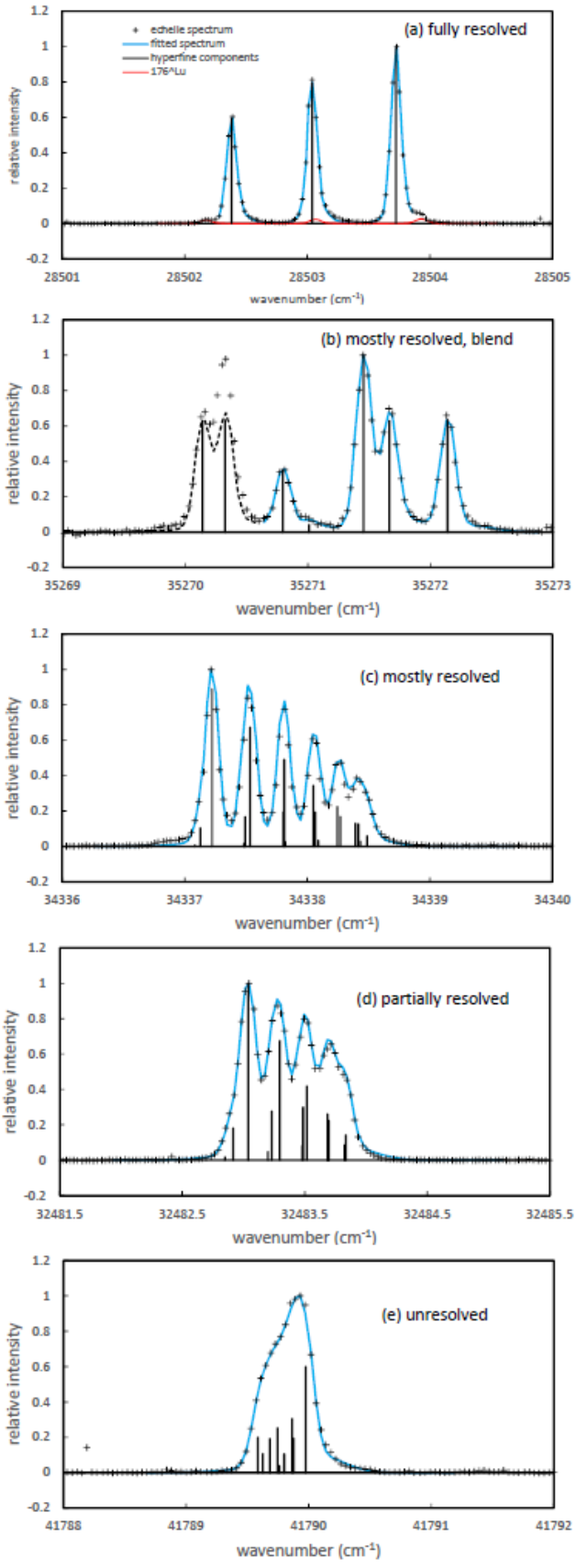
echelle spectrum
fitted spectrum
hyperfine components
176^Lu
(a) fully resolved
relative intensity
wavenumber (cm-1)
(b) mostly resolved, blend
(c) mostly resolved
(d) partially resolved
(e) unresolved

Figure 2.

Table 1. Transitions investigated in this study arranged by term-ordered upper level energy.

transition wavenumber[a] (cm^{-1})	wavelength in air[a] (Å)	Upper Level configuration and term	Upper Level E^a_{upper} (cm^{-1})	Lower Level configuration and term	Lower Level E^a_{lower} (cm^{-1})	line character[b]
28503.149	3507.38	6*s*6*p* $^3P^o_1$	28503.149	6*s*^{2} $^1S_0$	**0.000**	f
38223.49	2615.41	6*s*6*p* $^1P^o_1$	38223.49	6*s*^{2} $^1S_0$	**0.000**	p
25788.17	3876.65	6*s*6*p* $^1P^o_1$	38223.49	5*d*6*s* $^3D_2$	12435.32	m
29428.713	3397.07	5*d*6*p* $^3F^o_2$	41224.821	5*d*6*s* $^3D_1$	11796.108	m
28789.592	3472.48	5*d*6*p* $^3F^o_2$	41224.821	5*d*6*s* $^3D_2$	12435.229	u,bl[c]
23892.393	4184.25	5*d*6*p* $^3F^o_2$	41224.821	5*d*6*s* $^1D_2$	17332.428	m, bl[d]
32483.300	3077.61	5*d*6*p* $^3F^o_3$	44918.529	5*d*6*s* $^3D_2$	12435.229	p
30719.551	3254.32	5*d*6*p* $^3F^o_3$	44918.529	5*d*6*s* $^3D_3$	14198.978	p,bl[e]
34337.780	2911.39	5*d*6*p* $^3F^o_4$	48536.758	5*d*6*s* $^3D_3$	14198.978	m
33662.218	2969.82	5*d*6*p* $^1D^o_2$	45458.326	5*d*6*s* $^3D_1$	11796.108	m
31259.348	3198.12	5*d*6*p* $^1D^o_2$	45458.326	5*d*6*s* $^3D_3$	14198.978	m
28125.898	3554.43	5*d*6*p* $^1D^o_2$	45458.326	5*d*6*s* $^1D_2$	17332.428	p
45532.33	2195.56	5*d*6*p* $^3D^o_1$	45532.33	6*s*^{2} $^1S_0$	**0.000**	u[f]
33736.09	2963.32	5*d*6*p* $^3D^o_1$	45532.33	5*d*6*s* $^3D_1$	11796.24	m,bl[d]
33097.01	3020.54	5*d*6*p* $^3D^o_1$	45532.33	5*d*6*s* $^3D_2$	12435.32	m,bl[g]
35108.14	2847.51	5*d*6*p* $^3D^o_2$	46904.38	5*d*6*s* $^3D_1$	11796.24	m
34469.06	2900.30	5*d*6*p* $^3D^o_2$	46904.38	5*d*6*s* $^3D_2$	12435.32	m
32705.30	3056.72	5*d*6*p* $^3D^o_2$	46904.38	5*d*6*s* $^3D_3$	14199.08	m
36297.87	2754.17	5*d*6*p* $^3D^o_3$	48733.19	5*d*6*s* $^3D_2$	12435.32	m
34534.11	2894.84	5*d*6*p* $^3D^o_3$	48733.19	5*d*6*s* $^3D_3$	14199.08	m
38167.34	2619.26	5*d*6*p* $^3P^o_0$	49963.58	5*d*6*s* $^3D_1$	11796.24	m
38252.96	2613.40	5*d*6*p* $^3P^o_1$	50049.20	5*d*6*s* $^3D_1$	11796.24	m
37613.88	2657.80	5*d*6*p* $^3P^o_1$	50049.20	5*d*6*s* $^3D_2$	12435.32	m
39405.42	2536.96	5*d*6*p* $^3P^o_2$	51201.66	5*d*6*s* $^3D_1$	11796.24	m
38766.34	2578.79	5*d*6*p* $^3P^o_2$	51201.66	5*d*6*s* $^3D_2$	12435.32	m
37002.58	2701.71	5*d*6*p* $^3P^o_2$	51201.66	5*d*6*s* $^3D_3$	14199.08	m
33869.08	2951.68	5*d*6*p* $^3P^o_2$	51201.66	5*d*6*s* $^1D_2$	17332.58	p
38880.25	2571.23	5*d*6*p* $^1F^o_3$	53079.33	5*d*6*s* $^3D_3$	14199.08	m,bl[d]
35746.75	2796.63	5*d*6*p* $^1F^o_3$	53079.33	5*d*6*s* $^1D_2$	17332.58	p
41789.8	2392.20	5*d*6*p* $^1P^o_1$	59122.4	5*d*6*s* $^1D_2$	17332.58	u[h]
23470.3	4259.50	5*d*6*p* $^1P^o_1$	59122.4	5*d*^{2} $^3P_0$	35652.1	u[i]
36509.9	2738.17	6*s*7*s* $^3S_1$	63774.3	6*s*6*p* $^3P^o_0$	27264.40	f
35271.1	2834.35	6*s*7*s* $^3S_1$	63774.3	6*s*6*p* $^3P^o_1$	28503.16	m, bl[j]
43904.7	2276.96	6*s*6*d*? $^3D?_1$	71169.1	6*s*6*p* $^3P^o_0$	27264.40	u[f]
42665.9	2343.07	6*s*6*d*? $^3D?_1$	71169.1	6*s*6*p* $^3P^o_1$	28503.16	f

NOTES –

[a] See text for discussion regarding the source references for level energies. Transition wavenumbers are calculated from listed energies. Wavelengths are calculated from transition wavenumbers using the standard index of air from Peck & Reeder (1972).

[b] line character descriptions: f – fully resolved; m – mostly resolved; p – partially resolved; u – unresolved**; bl – blend**

[c] this line is severely blended by a large neon line on the red end. Consistent but inferior results, not used in final averages

[d] small blending line at one end of line pattern, does not affect fit

[e] blend on blue end partially obscuring line, fit made to three red-most peaks

[f] featureless line, width consistent with but not used in final average.

[g] blends on red and blue ends partially obscuring line, fit made to two red-most peaks

[h] unresolved but definite asymmetry to break sign degeneracy in A.

[i] featureless line in the midst of but resolved from unknown blend with very wide HFS, consistent but inferior results not used in final averages

[j] wide pattern with weak blend adding intensity to second-to-red-most line, fit made to four blue-most peaks

Table 2. HFS constants for levels of $^{175}Lu^{+}$.

configuration	term	E[a] (cm^{-1})	A (this study) (mK)[d]	B (this study) (mK)[d]	A[b] (mK)[d]	B[b] (mK)[d]	A[c] (mK)[d]	B[c] (mK)[d]
5*d*6*s*	$^3D_1$	11796.108	-68.5 ± 0.3	29.3 ± 1.0	-68.32 ± 0.07	29.3 ± 0.7	-68.23 ± 0.08	28.65 ± 0.45
6*s*6*p*	$^3P^o_1$	28503.149	165.5 ± 0.3	-62.4 ± 1.0	165.38 ± 0.07	-61.1 ± 0.7	165.47 ± 0.08	-60.59 ± 0.45
6*s*6*p*	$^1P^o_1$	38223.49	-37.4 ± 0.3	74 ± 3	…	…	…	…
5*d*6*p*	$^3F^o_2$	41224.821	27.1 ± 0.3	63 ± 3	26.95 ± 0.10	63.9 ± 1.0	…	…
5*d*6*p*.....	$^3F^o_3$	44918.529	10.8 ± 0.4	119 ± 10	10.9 ± 0.20	105.2 ± 2.0	…	…
5*d*6*p*	$^3F^o_4$	48536.758	3.3 ± 0.3	180 ± 10	2.9 ± 0.3	192 ± 4	…	…
5*d*6*p*	$^1D^o_2$	45458.326	2.0 ± 0.3	...	2 ± 1	-10 ± 5	…	…
5*d*6*p*	$^3D^o_1$	45532.33	12.7 ± 1.0	...	…	…	…	…
5*d*6*p*	$^3D^o_2$	46904.38	4.3 ± 0.3	28 ± 5	…	…	…	…
5*d*6*p*	$^3D^o_3$	48733.19	4.6 ± 0.3	-2 ± 4	…	…	…	…
5*d*6*p*	$^3P^o_1$	50049.20	10.8 ± 0.6	31 ± 3	…	…	…	…
5*d*6*p*	$^3P^o_2$	51201.66	-0.4 ± 0.4	14 ± 5	…	…	…	…
5*d*6*p*	$^1F^o_3$	53079.33	7.4 ± 0.3	134 ± 10	…	…	…	…
5*d*6*p*	$^1P^o_1$	59122.4	-3.9 ± 1.0	...	…	…	…	…
6*s*7*s*	$^3S_1$	63774.3	249.0 ± 1.0	1 ± 4	…	…	…	…
6*s*6*d*?	$^3D?$ J=1	71169.1	-9.8 ± 0.6	38 ± 9	…	…	…	…

NOTES –

[a] Energy levels to three digits past decimal are from Lawler et al. (2009). The remainder are taken from the NIST ASD (Kramida et al 2018).

[b] Sneden et al. (2003)

[c] Steudel (1958)

[d] 1 mK = 10^{-3} cm^{-1}

Table 3. Hyperfine structure line component patterns for 35 transitions of ^{175}Lu II.

wavenumber (cm^{-1})	wavelength in air (Å)	F_{upp}	F_{low}	component offset (cm^{-1})	component offset (Å)	component normalized strength
45532.33	2195.556	4.5	3.5	0.04445	-0.002144	0.41667
45532.33	2195.556	3.5	3.5	-0.01270	0.000612	0.33333
45532.33	2195.556	2.5	3.5	-0.05715	0.002756	0.25000
43904.70	2276.957	4.5	3.5	-0.02480	0.001286	0.41667
43904.70	2276.957	3.5	3.5	-0.01734	0.000900	0.33333
43904.70	2276.957	2.5	3.5	0.06446	-0.003343	0.25000
42665.94	2343.072	4.5	4.5	-0.58836	0.032314	0.25463
42665.94	2343.072	4.5	3.5	0.09694	-0.005324	0.16204
42665.94	2343.072	3.5	4.5	-0.58090	0.031904	0.16204
42665.94	2343.072	3.5	3.5	0.10439	-0.005733	0.01058
42665.94	2343.072	3.5	2.5	0.75960	-0.041717	0.16071
42665.94	2343.072	2.5	3.5	0.18619	-0.010226	0.16071
42665.94	2343.072	2.5	2.5	0.84140	-0.046210	0.08929

(This table is available in its entirety in a machine-readable form in the online journal. A portion is shown here for guidance regarding its form and content.)